Diffusion Equation and Distance Scaling Methods of Global Optimization: Applications to Crystal Structure Prediction

Ryszard J. Wawak, Jaroslaw Pillardy,† Adam Liwo,‡ Kenneth D. Gibson, and Harold A. Scheraga*

Baker Laboratory of Chemistry, Cornell University, Ithaca, New York 14853-1301

Received: July 24, 1997; In Final Form: December 19, 1997

Two methods of global minimization, the diffusion equation method and the distance scaling method, are applied to predict the crystal structures of the hexasulfur and benzene molecules. No knowledge about the systems other than the geometry of the molecules and the pairwise potentials is assumed; i.e., no assumptions are made about the space groups, cell dimensions, or number of molecules in the unit cell. Both methods are based on smoothing transformations of the original potential energy surface, which remove all insignificant local minima; the surviving minima are traced back to the original potential energy surface during the so-called reversing procedure, in which the transformations are gradually removed. The crystal structures, known from experiment, were predicted correctly. To verify the power of the methods, the problem of global minimization of the potential energy of crystals of both molecules was intentionally increased considerably in complexity: viz., the numbers of molecules in the unit cell were doubled (from three to six in the case of hexasulfur and from four to eight in the case of benzene), and the search for the global minimum was repeated; the method again located the global minimum for each molecule. Additionally, local minimizations starting from the lowest-energy structures were carried out with a pressure term included, leading to the observed high-pressure structure of benzene.

1. Introduction

The theoretical prediction of a crystal structure from a knowledge of only the structures of its constituent molecules has been thought to be an extremely difficult, if not an unsolvable, problem.[1−3] In general, the thermodynamically most stable structure should be located as the correct structure prediction; i.e., the structure with the lowest free energy should be identified. Since this is computationally impractical, a common simplification is to look for the global minimum of the potential energy. Despite many efforts,[4−15] the latter problem remains unresolved, or only partially resolved. The main obstacles in locating the most stable (global-minimum) crystal structure are the existence of numerous local minima of the potential energy of a structure and the high dimensionality of the potential energy surface (when no knowledge of space-group symmetry is assumed). Other serious obstacles include the large number of interatomic interactions that must be considered in the energy computations, the necessity to use the Ewald summation to calculate the electrostatic energy,[16−18] and the problem of the very definition of the energy of a crystal when the dipole moment of the unit cell is nonzero.[19−23]

The choice of the intermolecular potential also involves a difficult decision. There are many possible potential functions, differing in parametrization and in the shape of the potential energy function, described in the literature.[24] The choice of the potential in the case of crystal calculations is critical,[3,15,24,25] and a very sophisticated one, for example, one involving a distributed multipole analysis including electrostatic anisotropy, should perhaps be used for the best reproduction of experimental results.[25] However, in many computer simulations involving a large number of energy and gradient calculations, it is necessary to use a simpler but less expensive potential function, from the computational point of view. Reasonably good results in the description of crystal structures may also be obtained by expressing the nonbonded part of the potential in the Lennard-Jones 6−12 or Buckingham 6-exp forms, with electrostatic interactions represented as Coulombic interactions between point charges;[15,24,26] also, a simpler 6-exp potential without any electrostatic term may be used for a good description of lattice energies.[27,28] However, by using an improper potential, it can be expected that one might obtain artificial, nonobservable structures as minima of such a potential, that differences in energy between different structures may be very small,[15] and that even the energetic order of the resulting structures may differ.[15] Thus, effective methods of global optimization for crystal structures to locate low-energy structures can be used as an important tool for developing and parametrizing force fields. In the present paper, we use a Lennard-Jones 6−12 potential for hexasulfur[29,30] and the AMBER[31] potential for benzene molecules. These potentials have very simple functional forms, and they reproduce the experimental crystal structures satisfactorily; therefore, despite some inherent problems in them (e.g., they may not give the correct lattice energy), they were selected for this work.

One of the common simplifications of the theoretical crystal structure prediction problem is the use of space-group information,[3,13−15,32−34] which greatly reduces the number of variables. Another simplification is the introduction of information about the unit cell dimensions.[35,36] To the best of our

* To whom correspondence should be addressed.
† On leave from Department of Chemistry, Warsaw University, ul. Pasteura 1, 02-093 Warsaw, Poland.
‡ On leave from Department of Chemistry, University of Gdansk, ul. Sobieskiego 18, 80-952 Gdansk, Poland.

S1089-5639(97)02424-9 CCC: $15.00
Published on Web 04/07/1998

knowledge, ref 12 is the only work that does not use any such simplifications for theoretical crystal predictions. The Monte Carlo technique implemented in the MPA program of Williams[12] was used there to predict the crystal structures of benzene and urea, including the prediction of the space group symmetry and the number Z of molecules in the unit cell (calculations were carried out for 2 and 4 molecules in the unit cell, which correspond to 15 and 27 degrees of freedom, respectively, for both benzene and urea).

In the approach presented here, no knowledge about the unit cell or space-group symmetry is assumed; i.e., all molecules in the unit cell are allowed to move freely and independently as rigid bodies; only the geometry of the rigid molecules and the parameters of the pairwise interatomic potentials are taken as known. Since no space-group symmetry is assumed, the number of molecules Z in the unit cell and their relative positions must be predicted together with the cell parameters. Consequently, a global-optimization algorithm is applied for each reasonable number of molecules in the unit cell; the structure and the number of molecules corresponding to the lowest energy per molecule are predicted. To ensure that the method did not miss any important minima, and to test the power of the method, an additional *independent* global-minimum search is then carried out with twice as many molecules. If this additional search leads to the same structure as the previously computed lowest-energy one (represented by a superlattice with a unit cell twice as large as the predicted unit cell), then the predicted structure and the predicted value of Z are accepted. This additional search is a global optimization problem considerably more complex than the original one used for predicting the structure; in the case of benzene, for which $Z = 4$, this additional search was carried out with 8 molecules, which corresponds to 51 degrees of freedom. To our knowledge, there have been no previous attempts at global optimization of crystal systems with this complexity. The computational expense of one global minimization with a given number of molecules is equivalent to about 100 randomly started local minimizations of the original potential energy.

Multitrajectory versions of the diffusion equation method (DEM)[37−41] and of the distance scaling method (DSM)[42,43] are applied in this work for the crystal structure prediction. In both methods, the multidimensional potential energy surface is smoothed until only a few potential wells, the traces of the deepest minima of the original potential, remain. Those deepest minima are then recovered during the so-called reversing procedure, in which the deformation is gradually removed, and the predicted crystal structure is taken as the minimum with the lowest energy. Although the DEM and the DSM are applied here to pairwise potentials, they may also be used with multibody potentials, but this would require additional considerations.

Both methods are similar in that they are based on a consideration of trajectories of local minima that start from the minima on a highly deformed potential surface and are tracked back to the undeformed surface during the so-called reversing procedure. The lowest-energy local minima of the undeformed potential are among those obtained in that manner.

There are, however, some important differences between the two methods. In the DEM, the physical nature of the diffusion process leads to the smoothing of the potential surface; only a few local minima survive for strong deformations, and those minima are related to the lowest minima of the original potential. Mathematically, the smoothing arises from the convolution formula for the solution of the diffusion equation (eq 3), with the initial condition for solving the diffusion equation being the identification of the deformed surface at time zero with the complete undeformed surface.

In the case of the DSM, the smoothing of the potential energy surface is a result of deformation of the pairwise terms of which the complete energy function is constituted. The lowest local minimum of each pairwise potential is preserved while higher local minima are removed, and high-energy barriers are lowered; consequently, the potential energy surface becomes smoother and possesses fewer local minima.

Both methods were applied to predict the crystal structures of the S_6 molecule with the number of molecules in the unit cell ranging from one to six and of the benzene molecule, with one, two, three, four and eight molecules. In the case of S_6, both methods located the energy-minimized experimental structure in every computation. In addition, several artifacts with slightly lower energies were found in the computations with three, five, or six molecules. The term "artifact" is used here to designate a minimum-energy structure that probably cannot be observed experimentally, as described in Section 8. The results for S_6 molecules suggest that the globally minimized results may be used as a basis for verification of intermolecular force fields. In the case of benzene, the minimized experimental structure was found in the computations with four molecules and with eight molecules, and no lower-energy structures were located; also, no lower-energy structures were found in the computations with one, two, or three molecules at atmospheric pressure, supporting the prediction of $Z = 4$ as the correct one.

Compared to our earlier work,[41] the DEM has been extended to include the treatment of electrostatic interactions; in addition, for nonbonded interactions, the Gaussian approximation[38,41] of the transformed Lennard-Jones potential was replaced by a cubic spline approximation, which is more accurate, and 3−4 times less expensive computationally. For this reason, the computations for S_6 molecules were repeated, and the results are even better than in the earlier paper:[41] three previously missed structures of very low energy (lower than the energy of the minimized experimental structure) were now found in the computations with six molecules.

The DSM was applied successfully in previous work[42] to predict the global-minimum arrangements of argon clusters (a predecessor of the DSM, the shift method,[44,45] also correctly located the lowest-minimum structures of water clusters). The current work, the theoretical prediction of the crystal structures of the hexasulfur and benzene molecules, shows that the DSM is at least as suitable as the DEM for this problem. Moreover, the great advantage of the DSM is that it is easier to apply than the DEM.

2. Methods

The energy surface of the original potential function $f(\mathbf{u})$, $\mathbf{u}$ being a point in the multidimensional domain, usually possesses a number of local minima that grows exponentially with the dimension of the problem. The reason for applying the DEM or the DSM is to smooth this surface, to be able to use any standard local minimization procedure to locate the few local minima that survive in the deformed surface, and to trace them back to the deepest minima of the original potential function by using the so-called "reversing procedure". The position of a surviving local minimum in the deformed surface depends on the magnitude of the deformation, and, usually, differs from the position of this minimum in the undeformed surface. Thus, the goal of the reversing procedure is to recover the trajectory connecting all the positions of this minimum.

In the case of the DEM, the function $f(\mathbf{u})$ is treated as the initial condition for solving the diffusion equation, and the smoothed function $F(\mathbf{u}, t)$ is the solution of this equation, with t interpreted as time:

$$\Delta_{\mathbf{u}} F(\mathbf{u}, t) = \frac{\partial}{\partial t} F(\mathbf{u}, t) \qquad (1)$$

$$F(\mathbf{u}, 0) = f(\mathbf{u})$$

For a sufficiently large time T, referred to as the maximum-deformation time, the function $F(\mathbf{u}, T)$ has only a few local minima, which can easily be located by any strategy for global minimization, such as energy minimization or Monte Carlo with local minimization (MCM).[46,47]

In the case of the DSM, the transformation has a very simple algebraic form; it is the original formula, with the atom−atom distance r replaced by r', where

$$r' = \frac{r + r_0\alpha}{1 + \alpha} \qquad (2)$$

α is the deformation parameter, and r_0 is the minimum position for the pairwise interaction. Then, the transformed Lennard-Jones potential has the form $\epsilon[(r_0/r')^{12} - 2(r_0/r')^6]$, and the total transformed Lennard-Jones energy, U_{LJ}, is a sum of all such pairwise interactions. As follows from eq 2, the basin of the local minimum in the pairwise interaction increases with the parameter α, and consequently, the complete function, U_{LJ}, becomes smoother. Hence, the DSM deformation leads to a Lennard-Jones potential energy surface with only a few local minima for larger values of α, as in the case of the DEM. By contrast, however, to the DEM, where the system usually expands significantly for larger values of time, the size of the structures corresponding to the local minima for the DSM-transformed Lennard-Jones potential remains similar to the original size with the undeformed potential. Since the electrostatic interaction is always accompanied by a 6−12 Lennard-Jones one, the same mathematical formula (eq 2) is used for the transformation of r in the term $1/r$ as for the Lennard-Jones term.

Each of the local-minimum configurations for large deformations can then be traced back through the reversing procedure in which the deformation parameter is decreased in steps, i.e., the successive energy surfaces are closer to the original energy surface. Local minimizations at each step start from the local minima of the previous step or from perturbations of those minima. Gay's routine SUMSL,[48] a secant-type unconstrained minimization solver, was used for all local minimizations.

Before the reversing procedure starts, a search consisting of 100 local minimizations, starting from randomly generated points on the maximally deformed potential energy surface, is carried out. Because the number of minima for a highly deformed potential function is significantly less than the number of minima for an undeformed function, this search is highly effective and leads only to a few local minima. In addition, a local minimization on a highly deformed surface is 2−5 times faster than one carried out for an undeformed function. The reversing procedure applied in the present work was a multi-trajectory one; i.e., more than one local minimum from the maximally deformed surface was tracked back in the deformation to the undeformed surface. The number of minima tracked back was chosen as 8, and therefore, up to 8 of the lowest-energy minima resulting from 100 local minimizations were chosen for the reversing procedure. The reversing procedure consists of consecutive steps, each of them carried out at a different deformation parameter, so that the deformation parameter in the step is smaller than that in the previous step. Each reversing procedure step begins with local minimizations of up to eight of the lowest-energy structures found at the previous step. The number of resulting local minima is not greater than eight and may be less because different minima from the previous step may merge while changing the deformation parameter. Then, for each resulting local minimum, three random perturbations were carried out, in which all variables for a given structure (including lattice vectors) were changed randomly in the range of 20% of the original value, and the perturbed structures were minimized, producing up to 24 different minima. At the end of this step, there were up to 32 local minima, from which up to 8 lowest-energy structures were chosen for the next reversing-procedure step. Before the next step starts, the deformation parameter is decreased. For the DEM, the deformation parameter (diffusion time) changes according to a logarithmic scale, each time being divided by 2, and the reversing procedure is terminated when the deformation reaches the value of 10^{-8}. For the DSM, the deformation parameter changes linearly by decreasing it by 0.03 in each deformation step, and the reversing procedure ends when the deformation is equal to 0. There were no perturbations carried out for the undeformed function; only local minimizations were carried out, and the predicted crystal structure (including the value of Z) was taken as the one of lowest energy.

The value of the maximum-deformation time T in the DEM does not influence the result significantly if T is chosen large enough. Values of T ranging from 0.5 to 5.0 were examined and led to the same global minimum. In the crystal calculations, a change in the deformation parameter t results in changes in the energy and in the volume of the unit cell of each particular structure; for small values of t these changes occur rapidly with increasing t, whereas for larger values of t the energy and the volume of the unit cell stabilize. This value of time t is chosen as the maximum-deformation time T; in the present paper, the value of T was chosen as 1.0.

Similarly, the choice of the maximum-deformation parameter α_{max} in the DSM is not crucial; the results remain unchanged if this parameter is large enough; above a certain value of α, changes in the local-minima structures and their energies become small, and this value of α is chosen as α_{max}. The α_{max} parameter has been determined to be 0.3 for the hexasulfur and benzene computations.

3. The DEM Applied to Crystals of Rigid Molecules

As opposed to the DSM, whose application is straightforward, the implementation of the DEM requires a solution of eq 1. This can be done if the multidimensional Fourier−Poisson integral (the convolution of the function f, and a Gaussian-type function whose width depends on time t)

$$F(\mathbf{u}, t) = (2\sqrt{\pi t})^{-m} \int_{R^m} f(\mathbf{v}) \exp(-||\mathbf{u} - \mathbf{v}||^2/4t)\, d\mathbf{v} \qquad (3)$$

can be evaluated within a reasonable computer time, where m is the number of variables and $\mathbf{v}$ is the integration variable; the computation of the integral in eq 3 is described in the present section.

3.1. Tetrahedra as a Tool for Solving the Diffusion Equation. The application of the DEM in its rigorous original formulation would require that the diffusion equation be solved in the independent variables of the crystal energy function (the six parameters a, b, c, α, β, γ of the unit cell, three Eulerian

angles per molecule defining the relative orientation of the molecule with respect to the unit cell, and three translations for all molecules but one; the latter is a translationally fixed reference, removing the three translational degrees of freedom of the entire system). However, the Cartesian coordinates of the atoms belonging to the system, and, consequently, the interatomic distances and the energy, are very complicated functions of these variables. Since it is practically impossible to solve the diffusion equation in such variables, we have adopted another approach. The lattice vectors **a**, **b**, **c** are defined by nine Cartesian coordinates; the position of the center of mass and the orientation of each of the molecules M_1, M_2, ..., M_Z in the unit cell are defined by the Cartesian coordinates of the vertexes of an auxiliary regular tetrahedron associated with each particular molecule in the unit cell. For the molecule M_i, $i = 1, 2, ..., Z$, the associated regular tetrahedron Δ_i has a given size, the same for each molecule, with its center at the center of mass of M_i. Moreover, the vertexes of the tetrahedron Δ_i are treated as virtual atoms of the molecule M_i, so that they and the real atoms of M_i constitute a rigid structure. The position of any atom of the molecule M_i is a unique weighted sum of the positions of the vertexes of the tetrahedron Δ_i, and the weights of the sum remain constant even if the molecule is translated or rotated. Hence, the Cartesian *x*, *y*, *z*-coordinates of any atom of the molecule M_i in the unit cell are linear combinations of the Cartesian *x*, *y*, *z*-coordinates, respectively, of the vertexes of the tetrahedron Δ_i, with the constant coefficients of these linear combinations being the weights, the same for the *x*, *y*, and *z*-coordinates. Consequently, the Cartesian *x*, *y*, *z*-coordinates of an atom belonging to a molecule $M_i(n_a, n_b, n_c)$ (a translational image of M_i by the vector $n_a\mathbf{a} + n_b\mathbf{b} + n_c\mathbf{c}$), for any $i = 1, 2, ..., Z$ and any integer numbers n_a, n_b, n_c, are linear combinations of the *x*, *y*, *z*-coordinates of the vertexes of the tetrahedron Δ_i and the *x*, *y*, *z*-coordinates of the vectors **a**, **b**, **c**. Obviously, to maintain the shape of the molecule, the Cartesian coordinates of the vertexes of the tetrahedron must be correlated so that the vertexes constitute a regular tetrahedron of a given size.

At this point, we allow the Cartesian coordinates of the vertexes of tetrahedra Δ_1, Δ_2, ..., Δ_Z to assume any real values; i.e., we allow violations of the initially imposed constraints (regularity and size of the tetrahedra). The positions of all atoms, however, are calculated by using the same linear combinations as earlier, with the same unchanged coefficients. Consequently, if the constraints imposed on the tetrahedra are violated, the shapes of the corresponding molecules change. We treat all the Cartesian coordinates of the vertexes of Δ_1, Δ_2, ..., Δ_Z and all the Cartesian coordinates of the vectors **a**, **b**, **c**, as independent variables.

The total number of independent variables with 4 vertexes of each tetrahedron and 3 lattice vectors equals $12Z + 9$, and the physically acceptable geometries correspond to those points of R^{12Z+9} that satisfy the regularity and size constraints for tetrahedra Δ_1, Δ_2, ..., Δ_Z. These points constitute a $(6Z + 9)$-dimensional *submanifold* (six external degrees of freedom per tetrahedron and three lattice vectors) in the Cartesian $(12Z + 9)$-dimensional space.

To compensate for the violations of the imposed constraints, we solve the diffusion equation in R^{12Z+9} and observe its solution and carry out the reversing procedure and local minimizations on a $(6Z + 3)$-dimensional submanifold corresponding to the physically acceptable geometries, with the six degrees of freedom of the entire system being eliminated.

The great advantage of choosing the Cartesian coordinates of the vertexes of Δ_1, Δ_2, ..., Δ_Z and the Cartesian coordinates of the vectors **a**, **b**, **c**, as independent variables is that the Cartesian *x*, *y*, *z*-coordinates of any atom of any molecule are linear combinations of independent variables; this significantly simplifies the problem of solving the diffusion equation, as shown in the following subsection.

3.2. Interatomic Distances and Convolution. The original potential energy function is a sum (over lattice cells, molecules, and atoms) of pairwise contributions. Hence, according to eq 3, the solution of the diffusion equation is also a sum (over the same cells, molecules, and atoms), but the pairwise contributions are now the Fourier−Poisson integrals of pairwise terms replacing the complete energy function. Each of the pairwise terms is of the radial form (6−12 Lennard-Jones or electrostatic interactions in this study). Consequently, by using the tetrahedron approach, we need to calculate the Fourier−Poisson integrals over the Cartesian coordinates of the vertexes of only two tetrahedra (those associated with the two molecules whose atoms interact) and over the Cartesian coordinates of the lattice vectors **a**, **b**, **c**; in the situations in which an atom belonging to a molecule in the unit cell interacts with a nonunit cell atom belonging to a translational image of the same molecule, the Cartesian coordinates of the vertexes of only one tetrahedron and the vectors **a**, **b**, **c**, are used.

To calculate a Fourier−Poisson integral of pairwise terms, it is necessary to apply formulas for computing interatomic distances. As mentioned in the previous subsection, the *x*, *y*, *z*-coordinates of atom V of a molecule M_{i_V} (n_a^V, n_b^V, n_c^V) can be represented as the following linear combinations of independent variables

$$\begin{aligned} x_V &= d_1^V x_1^V + ... + d_4^V x_4^V + d_5^V x_5 + ... + d_7^V x_7 \\ y_V &= d_1^V y_1^V + ... + d_4^V y_4^V + d_5^V y_5 + ... + d_7^V y_7 \\ z_V &= d_1^V z_1^V + ... + d_4^V z_4^V + d_5^V z_5 + ... + d_7^V z_7 \end{aligned} \tag{4}$$

where the coefficients d_j^V with the indices $j \leq 4$ correspond to the vertexes of tetrahedron Δ_{i_V} (weights), whereas $d_5^V = n_a$, $d_6^V = n_b$, $d_7^V = n_c$. The independent variables *x*, *y*, *z* with indices ≤ 4 are the Cartesian coordinates of the four vertexes of Δ_{i_V}, and those with indices ≥ 5 are the Cartesian coordinates of the vectors **a**, **b**, **c** (they do not have the superscript "V" since they are the same independent variables for all atoms in the system). If W is another atom of the system, the square of the distance between V and W can be represented as

$$\begin{aligned} \mathrm{dist}^2(V, W) = [d_1^V x_1^V - d_1^W x_1^W + ... + d_4^V x_4^V - d_4^W x_4^W + \\ (d_5^V - d_5^W)x_5 + ... + (d_7^V - d_7^W)x_7]^2 + [d_1^V y_1^V - d_1^W y_1^W + ... + \\ d_4^V y_4^V - d_4^W y_4^W + (d_5^V - d_5^W)y_5 + ... + (d_7^V - d_7^W)y_7]^2 + \\ [d_1^V z_1^V - d_1^W z_1^W + ... + d_4^V z_4^V - d_4^W z_4^W + (d_5^V - d_5^W)z_5 + ... + \\ (d_7^V - d_7^W)z_7]^2 \end{aligned} \tag{5}$$

If $i_V \neq i_W$, then all the *x*, *y*, *z* variables in eq 5 are independent variables. If $i_V = i_W$ (i.e., V and W belong to translational images of the same molecule), the variables x_1^V, x_2^V, x_3^V, x_4^V coincide with the variables x_1^W, x_2^W, x_3^W, x_4^W, respectively, and the same coincidence holds for the variables *y* and *z*. In this case

$$\mathrm{dist}^2(\mathrm{V},\mathrm{W}) = [(d_1^{\mathrm{V}} - d_1^{\mathrm{W}})x_1^{\mathrm{V}} + ... + (d_4^{\mathrm{V}} - d_4^{\mathrm{W}})x_4^{\mathrm{V}} + (d_5^{\mathrm{V}} - d_5^{\mathrm{W}})x_5 + ... + (d_7^{\mathrm{V}} - d_7^{\mathrm{W}})x_7]^2 + [(d_1^{\mathrm{V}} - d_1^{\mathrm{W}})y_1^{\mathrm{V}} + ... + (d_4^{\mathrm{V}} - d_4^{\mathrm{W}})y_4^{\mathrm{V}} + (d_5^{\mathrm{V}} - d_5^{\mathrm{W}})y_5 + ... + (d_7^{\mathrm{V}} - d_7^{\mathrm{W}})y_7]^2 + [(d_1^{\mathrm{V}} - d_1^{\mathrm{W}})z_1^{\mathrm{V}} + ... + (d_4^{\mathrm{V}} - d_4^{\mathrm{W}})z_4^{\mathrm{V}} + (d_5^{\mathrm{V}} - d_5^{\mathrm{W}})z_5 + ... + (d_7^{\mathrm{V}} - d_7^{\mathrm{W}})z_7]^2 \quad (6)$$

where all the x, y, z variables in eq 6 are independent variables.

Consequently, a pairwise interaction (of the original potential function) has the form $f(d_1x_1 + ... + d_kx_k, d_1y_1 + ... + d_ky_k, d_1z_1 + ... + d_kz_k)$, i.e., is a radial function of a linear combination of k vectors in R^3. The Fourier−Poisson integral for this interaction is the convolution of f and a product of $3k$ identical normalized Gaussian-type functions g, each in one of the variables x_1, ..., x_k, y_1, ..., y_k, z_1, ..., z_k; the width of the Gaussian g is the same as the width of the Gaussian in eq 3 [defined by the factor $1/(4t)$]. It can be shown (ref 49, section 20) that this convolution can be represented by a simpler formula

$$f(X, Y, Z)*[G(X)\,G(Y)\,G(Z)](d_1x_1 + ... + d_kx_k, d_1y_1 + ... + d_ky_k, d_1z_1 + ... + d_kz_k) \quad (7)$$

where

$$G(X) = (g_{d_1}*...*g_{d_k})(X) \quad \text{and} \quad g_{d_j}(\xi) = \frac{g(\xi/|d_j|)}{|d_j|} \quad (8)$$

The functions $G(X)$, and likewise $G(Y)$, $G(Z)$, are also normalized Gaussian-type functions

$$G(X) = \frac{1}{t_e\sqrt{\pi}} \exp\left(-\frac{X}{t_e}\right)^2 \quad (9)$$

where $t_e = [4t(d_1^2 + ... + d_K^2)]^{1/2}$; t_e will be called the effective time for a pairwise interaction. In other words, the $3k$-dimensional convolution is being replaced by a 3-dimensional convolution of the function $f(X, Y, Z)$ with a Gaussian-type function $G(X)\,G(Y)\,G(Z)$ where the width of G depends on the time t and also on the coefficients d_j of the linear combinations associated with the pair of atoms in the pairwise interaction. Since the function f is radial, the three-dimensional convolution can easily be reduced to a one-dimensional convolution by using spherical coordinates in the calculation of the convolution in eq 7.

3.3. One-Dimensional Convolutions with Gaussian-Type Functions. The 6−12 Lennard-Jones contribution in a pairwise interaction leads to one-dimensional convolutions of the functions $1/r^5$ and $1/r^{11}$ with a Gaussian (the change in the power of r is due to the substitution of spherical coordinates for the spatial x, y, z-coordinates in the calculations of the convolution in eq 7 for the Lennard-Jones term, which introduces a multiplication by the Jacobian of this substitution). These functions are not locally integrable in the neighborhood of $r = 0$ (i.e., the area of the region restricted by the functions $1/r^5$ or $1/r^{11}$ and both axes of a two-dimensional coordinate system is infinite in any neighborhood of zero distance); hence, to apply the DEM, the Lennard-Jones functions have to be redefined for small interatomic distances so that they are bounded functions. The corresponding one-dimensional functions convolved with a Gaussian-type function cannot be represented by an analytical formula. For this reason, approximations of the convolutions are used. Previously,[38,40] a sum of two Gaussian-type functions was used to approximate the Lennard-Jones potential; this led to analytical formulas for the one-dimensional convolutions. However, in the case of crystal structures, where high accuracy is required for both small and large interatomic distances, it was necessary to use as many as six Gaussian-type terms,[41] which was computationally expensive. In the current work, the one-dimensional convolutions are represented by cubic splines, as shown below.

First, 2000 points on the positive axis are chosen: $p_i = p_0q^i$, for $i = 1, 2, ..., 2000$, where $q^{100} = 2$ (the significance of this equality will be explained later), and $p_0 = 0.1$. Then, the functions $1/r^5$ and $1/r^{11}$ are redefined to constant values equal to $1/p_0{}^5$ and $1/p_0{}^{11}$ respectively, for $r < p_0$; i.e., the assigned functions are bounded functions. Each of these functions is then approximated by linear functions in all intervals (p_{i-1}, p_i) for $i = 1, 2, ..., 2000$; the new function is continuous, but its first derivative is not continuous at the points p_i. It is then convolved with the Gaussian $(1/\sqrt{\pi})\exp(-r^2)$, by calculating analytically and summing up all the convolutions of the linear approximations in the intervals (p_{i-1}, p_i) with the Gaussian. The resulting functions (one for $1/r^5$ and one for $1/r^{11}$) are continuous functions, and now all the derivatives are continuous (ref 49 section 15). These two functions are then approximated by cubic splines[50] based on the values of the functions at the points p_i, $i = 0, 1, 2, ..., 2000$, and their coefficients are precalculated. The two cubic splines are then used to evaluate the Lennard-Jones function transformed according to the diffusion equation method, by calculating the cubic splines for $1/r^5$ and $1/r^{11}$ for the variable $R = r/(4t_e)^{1/2}$ (t_e being the effective time for a pairwise interaction defined in subsection 3.2) and by dividing them by $r[(4t_e)^{1/2}]^5$ and $r[(4t_e)^{1/2}]^{11}$, respectively.

To avoid the expensive computations of the square root of the squared distance between two atoms, the actual computations are carried out for the squared variable R^2 in terms of the polynomial $a_3R^6 + a_2R^4 + a_1R^2 + a_0$, whose coefficients depend on the index i of the interval (p_{i-1}, p_i) such that $p_{i-1}^2 < R^2 \le p_i^2$. The p_i's for the cubic spline form a geometric series; this choice of the p_i's was made to be able to achieve high accuracy of the spline approximation for all distances, including very small and very large ones, with a small amount of precalculated coefficients. A straightforward way to locate the index would involve an expensive computation of the logarithm of R^2; instead, the binary computer representation of numbers is exploited by utilizing the fact that $q^{100} = 2$.

This approach saves about 70−80% of the computer time compared to the six-term Gaussian approximation. The spline approximation is accurate for distances larger than the local minimum distance of the transformed Lennard-Jones potential and is satisfactory for all distances that have a chance of being reached during local minimizations.

The electrostatic term also attains an infinite value for zero distance; however, the function $1/r$ is a locally integrable function in R^3. Hence, in contrast to the Lennard-Jones potential function, it can be treated explicitly without being redefined in the neighborhood of $r = 0$. The one-dimensional convolution used to calculate the transformed electrostatic term is proportional to a convolution of the function sign(r) and a Gaussian, which is represented analytically by a function $\mathrm{erf}(r/8t_e)/r$, where t_e is the effective time; i.e., after transformation by the Fourier−Poisson integral, $1/r$ becomes $\mathrm{erf}(r/8t_e)/r$.

4. Lattice Summation

A precise calculation of the energy of a crystal involves an infinite number of terms. In practical computations, a distance cutoff must be applied for the interactions between the atoms

in the unit cell and the non-unit-cell atoms. In this work, this is done by carrying out the lattice summations for only several layers of lattice cells surrounding the unit cell (usually 2−5 layers are realistic from the point of view of the computational time). However, to achieve reasonable accuracy (about 99% or more), the pairwise interactions must be functions that converge fast enough to zero for large distances. Moreover, since the same crystal lattice can be represented equivalently by different unit cells, a cell chosen for the computations should have a shape that is close to a cube; cells that are long in one direction and thin in another would require more layers in the computations to give the same accuracy. A practical way to achieve a high accuracy is to use the reduced cell based on the three shortest noncoplanar vectors connecting the points of the computed lattice.

The DEM- and the DSM-transformed Lennard-Jones and electrostatic interactions exhibit the same asymptotical behavior for large distances as the original interactions, i.e., the order of convergence to zero is $1/r^6$ for the transformed Lennard-Jones interactions and $1/r$ for the transformed electrostatic interactions. The Lennard-Jones contribution can be calculated in a straightforward way, as opposed to the electrostatic contribution, because of the very slow convergence of the function $1/r$ to zero. Therefore, the Ewald method[16−18] is usually used to calculate the electrostatic energy of a crystal, both when the molecule has a dipole moment and when it does not have one.[29,30]

The Ewald method is based on the use of the Fourier transformation and the Parseval formula (ref 49, section 17). The electrostatic energy is calculated as

$$E_{el} = E_d + E_r + E_c \tag{10}$$

where

$$E_d = \frac{1}{2}\sum_{i,j}^{M'}\sum_{n_a,n_b,n_c} q_i q_j \frac{\mathrm{erfc}(\alpha r_{i,j,n_a,n_b,n_c})}{r_{i,j,n_a,n_b,n_c}}$$

$$E_r = \frac{1}{2\pi V}\sum_{(m_a,m_b,m_c)\neq(0,0,0)} \frac{\exp(-(\pi\mathbf{m}/\alpha)^2)}{\mathbf{m}^2} \times \{[\sum_{i=1}^{M} q_i \cos(2\pi\mathbf{m}\cdot\mathbf{r}_i)]^2 + [\sum_{i=1}^{M} q_i \sin(2\pi\mathbf{m}\cdot\mathbf{r}_i)]^2\}$$

$$E_c = \frac{-\alpha}{\sqrt{\pi}}\sum_{i=1}^{M} q_i^2 \tag{11}$$

The prime over M (the number of atoms in the unit cell) denotes that $i \neq j$ if n_a, n_b, $n_c = 0$, i.e., if the atoms i and j lie in the unit cell. V is the volume of the original unit cell, $\mathbf{r}_i$ and $\mathbf{r}_j$ are the Cartesian coordinates of atoms i and j, respectively, in the unit cell, q_i and q_j are the respective charges, r_{i,j,n_a,n_b,n_c} is the distance from atom i in the unit cell to the image of atom j in the cell n_a, n_b, n_c, $\mathbf{m}$ is the linear combination of reciprocal vectors $\tilde{\mathbf{a}}$, $\tilde{\mathbf{b}}$, $\tilde{\mathbf{c}}$ with m_a, m_b, m_c as coefficients; the parameter α is chosen to ensure the fastest convergence of the sums in eq 11 by estimating the maximum errors in the computations of E_d and E_r from eq 11, for a given size of the unit cell and for a number of values of α. In the case in which rigid molecules are considered, the intramolecular interactions of the molecules in the unit cell are not included.

To apply the Ewald method to the DEM-transformed electrostatic potential, $\mathrm{erf}(r/8t_e)/r$, the latter is represented as $1/r - (1/r)\,\mathrm{erfc}(r/8t_e)$. The term $(1/r)\,\mathrm{erfc}(r/8t_e)$ converges rapidly to zero for large distances and can be calculated directly as is the Lennard-Jones function. The term $1/r$ is calculated using the standard Ewald method. All the summations over the real and over the reciprocal lattices are carried out by summing up over layers of unit cells or reciprocal unit cells, respectively.

Similarly, in the case of the DSM, the function $(1 + \alpha)/r$ must be subtracted from the transformed pairwise potential $(1 + \alpha)/(r + r_0\alpha)$ and added later as a separate term. The resulting difference of the functions converges to zero as the function $1/r^2$. Hence, when the charges in each unit cell sum to zero, the interactions between such unit cells exhibit a $1/\rho^4$ asymptotic behavior, where ρ is the distance between the centers of the interacting unit cells. The function $1/\rho^4$ is unconditionally convergent in R^3, and consequently, the difference of the functions can be treated directly in the real lattice summation, whereas the standard Ewald[16−18] method is applied for the remaining $(1 + \alpha)/r$ term.

TABLE 1: Parameters of Potential Functions[a]

atom type	ϵ (kcal/mol)	r_0 (Å)	q (electronic charge units)
S	0.805	3.66	0.00
C	0.120	3.70	−0.15
H	0.010	3.08	0.15

[a] For the Lennard-Jones potential, $E_{LJ} = \epsilon[(r_0/r)^{12} - 2(r_0/r)^6]$, and for the electrostatic energy $E_{el} = 332.09\ q_1q_2/r$ in kcal/mol.

5. Applications

Both methods are applied to predict the crystal structures of S_6 and benzene molecules. The molecules are assumed to be rigid. The sulfur atoms of different S_6 molecules interact according to a 6−12 Lennard-Jones potential. In the case of benzene, both 6−12 Lennard-Jones and Coulombic contributions are present (even though benzene has no dipole moment, the C and H atoms carry partial charges). The parameters of the potentials for hexasulfur[29,30] and benzene[31] (AMBER force field) are presented in Table 1. The length of the S−S bond in the hexasulfur molecule is equal to 2.057 Å, and consecutive bonds make an angle of 102.18°. The geometry of the benzene molecule was taken from AMBER;[31] the C−C and C−H bonds have lengths of 1.400 Å and 1.080 Å, respectively, and the bond angles are 120°.

The methods are applied with different values for the number of molecules in the unit cell. Since there is no a priori knowledge about Z, its value is also a result of the computations, so that Z is also a predicted value, for which the global minimum of the energy per molecule is the smallest.

When the potentials adopted here are used to minimize the energies of the experimental structures of the hexasulfur and benzene crystals, slight deviations are observed. Therefore, the target structures for the crystals studied here are those that result from a minimization of the experimental crystal structures (see footnote *a* in Tables 2−5).

6. Results and Discussion

The results of the application of the DEM and the DSM to hexasulfur and benzene molecules are presented in Tables 2−5. Since the computations with different numbers of molecules frequently lead to superlattices and sublattices of the same crystal structure, the tables include "standard equivalence matrixes", which define transformations from one realization to another. A detailed explanation of the use of the standard equivalence matrices is presented in Appendix A. The conventional lattices corresponding to the calculated structures along with their probable space-group symmetry are listed in Tables

TABLE 2: Parameters of Calculated Structures for S_6 Crystals Using the DEM[a]

Z	n[b]	a (Å)	b (Å)	c (Å)	α (deg)	β (deg)	γ (deg)	energy (kcal/mol)	volume of unit cell (Å^3/mol)	equivalence indicator[c]	standard equivalence matrix[d,e]		
3	1	5.588	8.493	8.614	95.47	103.30	104.27	−46.04	126.84		1	0	0
											0	1	0
											0	0	1
	2	5.560	8.528	8.558	95.83	103.42	101.79	−45.86	127.20		1	0	0
											0	1	0
											0	0	1
	3	***6.369***	***8.010***	***8.010***	***95.07***	***75.00***	***104.99***	***−45.81***	***127.08***		***2/3***	***1/3***	***−1/3***
											−1/3	***1/3***	***−4/3***
											1/3	***2/3***	***4/3***
	4	6.880	7.034	8.552	73.57	81.12	75.45	−45.73	127.57		1	0	0
											0	1	0
											0	0	1
	5	6.889	7.000	8.497	75.30	81.73	76.07	−45.54	127.73		1	0	0
											0	1	0
											0	0	1
	6	5.518	8.413	8.511	82.91	99.12	83.63	−45.41	127.90		1	0	0
											0	1	0
											0	0	1
	7	6.725	6.998	8.554	101.84	96.70	77.34	−45.34	127.79		1	1	−1
											−1	1	0
											1	0	1
6	1	8.493	8.614	11.175	103.30	75.73	84.52	−46.06	126.84	$Z = 3$, $n = 1$	0	1	0
											0	0	−1
											−2	0	0
	2	8.499	8.598	10.884	88.81	74.79	84.08	−45.94	127.15		1	0	0
											0	1	0
											0	0	1
	3	8.498	8.573	10.917	74.34	87.33	84.91	−45.90	127.11		1	0	0
											0	1	0
											0	0	1
	4	***6.369***	***10.774***	***11.451***	***101.90***	***86.29***	***97.10***	***−45.82***	***127.08***	***Z = 3, n = 3***	***2/3***	***1/3***	***−1/3***
											−1/3	***1/3***	***7/3***
											0	***−1***	***1***
	5	7.820	10.935	11.106	119.34	109.10	90.19	−45.61	127.77		−1/2	−1/2	−1
											1	0	0
											0	−1	1
	6	8.497	8.558	10.940	89.06	104.65	95.26	−45.55	127.56	$Z = 3$, $n = 5$	0	0	−1
											−1	1	0
											1	1	0

[a] Minimized experimental structure found by the DEM is shown with bold italic font, in a different, but equivalent, representation from the one usually used; see section 6 and also footnotes *d* and *e*. [b] The number of the successive lowest-energy local-minimum structure for given *Z*. [c] Shows equivalent unit cell with lowest possible *Z* in the present Table. [d] The lattice vectors in the current line can be expressed as linear combinations of the lattice vectors of the probable lattice (shown in Table 6) with the elements of the standard equivalence matrix; i.e, the product of the lattice vectors from Table 6 and the standard matrix produces a set of lattice vectors whose parameters are very close to those in the current line. [e] For an example of how to show the agreement between the lattice parameters of the equivalent structures, see Appendix A.

6 and 7 for hexasulfur and benzene, respectively; the standard equivalence matrices in Tables 2−5 show how the calculated lattices are derived from the corresponding conventional lattices.

Sulfur-6 crystallizes in the rhombohedral space group $R\bar{3}$, with one molecule in the unit cell, whose lattice parameters[51] are $a' = 6.407$ Å and $\alpha' = 115.19°$. After energy minimization, these values become[41] $a' = 6.370$ Å and $\alpha' = 116.22°$. This minimized structure can also be represented as a crystal with three molecules in a trigonal unit cell[41] (the first, $R\bar{3}$, structure in Table 6).

Without assuming any of this information, the DEM algorithm was carried out with three and with six molecules of S_6. Previously, the minimized experimental structure was found as the lowest-energy structure with one, two, four, or five molecules;[41] with three molecules, a lower energy artifact was found,[41] but this was not found with six molecules. For this reason, we repeated the computations only with three and six molecules using the new, more accurate approximation of the transformed Lennard-Jones potential function with cubic splines (see section 3.3). With three molecules, the DEM located the structure (shown in bold italic font in Table 2), which is equivalent to the trigonal unit cell of the minimized experimental structure; in addition, the method located two lower-energy artifacts. The artifact with the lowest energy (see Table 2, $Z = 3$, $n = 1$) had been found[41] previously. With six molecules the problem of global minimization becomes very challenging, but the DEM found a superlattice of the lowest-energy artifact[41] ($Z = 3$, $n = 1$) as the lowest-energy minimum. As in the earlier work,[41] the minimized experimental structure (as a duplication of $Z = 3$, $n = 3$) was found; a duplication of another low-energy artifact ($Z = 3$, $n = 5$) was also obtained. In addition, two new low-energy structures ($Z = 6$, $n = 2$ and $Z = 6$, $n = 3$), lower in energy than the minimized experimental one, were located; they are also artifacts.

In general, the results for S_6 molecules are a repetition of our earlier results[41] to a certain extent. Since our current algorithm is much faster than its earlier version, it was possible to increase the size of the perturbations in the reversing procedure (see section 2); this sometimes results in an increase in the number of iterations in the local minimizations and may be more time-consuming. However, the modified DEM seems to be even more powerful than its previous version,[41] and the

TABLE 3: Parameters of Calculated Structures for C_6H_6 Crystals Using the DEM[a]

Z	n[b]	a (Å)	b (Å)	c (Å)	α (deg)	β (deg)	γ (deg)	energy (kcal/mol)	volume of unit cell (Å^3/mol)	equivalence indicator[c]	standard equivalence matrix[d,e]		
1	1	4.860	4.860	4.860	93.49	93.49	86.52	−11.91	114.21		−1/3	1/3	1/3
											2/3	1/3	1/3
											1/3	2/3	−1/3
	2	5.199	5.199	5.255	77.84	102.16	64.27	−11.73	117.49		1/2	1/2	0
											−1/2	1/2	0
											0	0	1
2	1	5.511	6.264	6.751	90.00	90.00	73.12	−13.78	111.50		−1	0	0
											−1	0	−1
											0	−1	0
	2	5.421	5.496	7.641	90.00	74.07	90.00	−13.51	109.47		1	0	0
											0	−1	0
											0	0	−1
	3	5.487	6.374	7.163	90.00	90.00	64.52	−12.63	113.08		1	0	0
											0	0	−1
											0	1	0
3	1	5.412	9.190	9.190	63.76	101.32	78.68	−12.74	126.88		0	0	−1
											−1/3	1/3	−1/3
											1/3	2/3	1/3
	2	5.355	6.283	10.674	81.69	89.74	71.98	−12.71	112.53		1	0	0
											0	1	0
											0	0	1
	3	5.412	5.416	11.901	89.21	81.05	87.22	−12.67	114.72		1	0	0
											0	1	0
											0	0	1
4	***1***	***6.605***	***7.431***	***9.167***	***90.00***	***90.00***	***90.00***	***−13.88***	***112.49***		***0***	***0***	***1***
											1	***0***	***0***
											0	***1***	***0***
	2	6.265	8.714	8.714	101.55	100.58	100.58	−13.79	111.50	$Z = 2$, $n = 1$	−1	0	−1
											1	1	0
											1	−1	0
	3	7.719	7.719	8.065	73.18	106.82	89.21	−13.51	109.47	$Z = 2$, $n = 2$	−1	−1	0
											1	−1	0
											1	0	1
8	***1***	***7.432***	***11.298***	***11.298***	***71.53***	***90.00***	***90.00***	***−13.88***	***112.48***	***Z = 4, n = 1***	***−1***	***0***	***0***
											0	***1***	***1***
											0	***1***	***−1***
	2	9.753	9.753	11.021	112.23	112.23	87.62	−13.79	111.50	$Z = 2$, $n = 1$	0	1	1
											0	−1	1
											2	0	0

[a] Minimized experimental structure found by the DEM is shown with bold italic font, in a different, but equivalent, representation from the one usually used; see Section 6 and also footnotes *d* and *e*. [b] The number of the successive lowest-energy local-minimum structure for given *Z*. [c] Shows equivalent unit cell with lowest possible *Z* in the present table. [d] The lattice vectors in the current line can be expressed as linear combinations of the lattice vectors of the probable lattice (shown in Table 7) with the elements of the standard equivalence matrix; i.e, the product of the lattice vectors from Table 7 and the standard matrix produces a set of lattice vectors whose parameters are very close to those in the current line. [e] For an example of how to show the agreement between the lattice parameters of the equivalent structures, see Appendix A.

current application revealed the lowest-energy (artifact) with six molecules, whereas the previous application reached only the minimized experimental structure with this number of molecules.

The DSM algorithm was applied with a number of S_6 molecules ranging from one to six. With one, two, or four molecules, the minimized experimental structure was found as the lowest-energy structure. This structure was also found with three molecules, together with two lower-energy artifacts, the same as those located by the DEM. With six molecules, the DSM found the same superlattice of the lowest-energy artifact (see Table 4, $Z = 3$, $n = 1$) as the lowest-energy minimum, and a superlattice of the minimized experimental crystal structure ($Z = 3$, $n = 3$); the latter structure is the trigonal lattice corresponding to the minimized experimental crystal structure with one molecule ($Z = 1$, $n = 1$ in Table 4). In addition, the method found two other artifacts, specific for six molecules ($Z = 6$, $n = 2$ and $Z = 6$, $n = 3$). With five molecules, the minimized experimental structure was found as the third lowest-energy structure, together with two artifacts ($Z = 5$, $n = 1$; $Z = 5$, $n = 2$) of slightly lower energies, specific for this number of molecules. As shown in Table 4, many of the low-energy structures obtained with lower numbers of molecules are also located with higher numbers of molecules, which strongly indicates that the DSM reached all or almost all of the deepest local minima of the potential.

As a prediction of the crystal structure, the lowest-energy structure from Table 4 should be chosen provided that it is physically realistic; when two structures have the same lowest energy, the one of the smaller numbers of molecules should be chosen. As Table 4 indicates, the lowest energy per molecule is obtained with three molecules ($Z = 3$, $n = 1$) and with six molecules ($Z = 6$, $n = 1$), and these represent the same lattice. On this basis, the structure $Z = 3$, $n = 1$ should be chosen as the prediction of the crystal structure. However, as discussed in Section 8, this structure probably could not exist physically. The minimized experimental structure is found as one of the lowest- (but not the lowest-) energy structures of this potential. The fact that so many artifacts were found by both global-energy minimization methods shows how powerful these methods are.

TABLE 4: Parameters of Calculated Structures for S_6 Crystals Using the DSM[a]

Z	n[b]	a (Å)	b (Å)	c (Å)	α (deg)	β (deg)	γ (deg)	energy (kcal/mol)	volume of unit cell (Å^3/mol)	equivalence indicator[c]	standard equivalence matrix[d,e]		
1	***1***	***3.765***	***6.369***	***6.370***	***116.23***	***101.34***	***101.34***	***−45.79***	***127.10***		***0***	***0***	***−1***
											−1/3	***−2/3***	***1/3***
											−1/3	***1/3***	***1/3***
	2	3.769	6.362	6.362	117.75	106.17	73.83	−45.62	127.67		0	0	1
											−1/2	−1/2	0
											1/2	−1/2	0
	3	4.189	5.705	6.182	67.67	70.36	88.65	−45.31	127.80		1	0	0
											0	1	0
											0	0	1
	4	4.990	4.990	5.603	105.62	105.62	83.27	−44.72	129.22		1/2	−1/2	0
											1/2	1/2	0
											0	0	1
2	***1***	***6.369***	***6.369***	***7.526***	***101.36***	***78.64***	***63.78***	***−45.80***	***127.09***	***Z = 1, n = 1***	***−1/3***	***−2/3***	***1/3***
											1/3	***−1/3***	***−1/3***
											0	***0***	***2***
	2	6.031	6.798	6.848	90.00	90.00	65.41	−45.62	127.64		1	0	0
											0	0	−1
											0	1	0
	3	6.382	6.382	7.098	90.00	90.00	117.87	−45.56	127.77		1/2	1/2	0
											−1/2	1/2	0
											0	0	1
	4	6.193	6.631	7.157	103.41	84.82	66.04	−45.32	127.79	$Z = 1$, $n = 3$	−1	0	1
											0	−1	1
											1	1	0
	5	6.209	6.209	7.059	85.53	94.47	106.31	−44.21	129.96		1/2	1/2	0
											−1/2	1/2	0
											0	0	1
	6	5.763	6.380	8.136	77.63	94.84	65.35	−43.93	130.22		−1	0	0
											0	1	0
											0	0	−1
3	1	5.588	8.493	8.614	95.47	103.30	104.27	−46.04	126.84		1	0	0
											0	1	0
											0	0	1
	2	5.560	8.528	8.558	95.83	103.42	101.79	−45.86	127.20		1	0	0
											0	1	0
											0	0	1
	3	***6.730***	***6.730***	***8.850***	***86.38***	***86.38***	***106.95***	***−45.81***	***127.08***	***Z = 1, n = 1***	***1/3***	***2/3***	***2/3***
											1/3	***−1/3***	***2/3***
											2/3	***1/3***	***−5/3***
	4	6.880	7.034	8.552	73.57	81.12	75.45	−45.73	127.57		1	0	0
											0	1	0
											0	0	1
	5	6.363	6.429	10.002	84.12	97.47	72.69	−45.65	127.65	$Z = 1$, $n = 2$	1/2	1/2	0
											1/2	−1/2	1
											0	−1	−2
	6	6.889	7.000	8.497	75.30	81.73	76.07	−45.54	127.73		1	0	0
											0	1	0
											0	0	1
	7	6.725	6.998	8.554	78.16	96.70	102.66	−45.34	127.79	$Z = 1$, $n = 3$	−1	−1	1
											−1	1	0
											−1	0	−1
4	***1***	***6.369***	***7.526***	***11.451***	***109.18***	***86.29***	***101.35***	***−45.81***	***127.08***	***Z = 1, n = 1***	***−1/3***	***−2/3***	***1/3***
											0	***0***	***−2***
											1	***0***	***1***
	2	6.429	7.537	11.307	79.83	88.47	108.09	−45.66	127.65	$Z = 1$, $n = 2$	−1/2	1/2	−1
											0	0	2
											1/2	3/2	1
	3	6.358	7.536	11.655	71.14	94.83	105.09	−45.62	127.55		1	0	0
											0	0	2
											0	−1	1
	4	7.157	8.577	8.820	103.64	96.46	76.72	−45.34	127.78	$Z = 1$, $n = 3$	1	1	0
											2	0	−1
											−1	1	−1
5	1	8.005	8.006	10.783	73.44	73.45	95.18	−45.93	126.96		1	0	0
											0	1	0
											0	0	1
	2	6.796	8.516	11.325	85.73	78.70	82.39	−45.82	127.24		1	0	0
											0	1	0
											0	0	1

TABLE 4 (Continued)

Z	*n*[b]	*a* (Å)	*b* (Å)	*c* (Å)	α (deg)	*β* (deg)	*γ* (deg)	energy (kcal/mol)	volume of unit cell (Å^3/mol)	equivalence indicator[c]	standard equivalence matrix[d,e]		
	3	***6.739***	***8.848***	***11.440***	***69.92***	***83.02***	***86.51***	***−45.80***	***127.17***	***Z = 1, n = 1***	***1/3***	***2/3***	***2/3***
											−1/3	***1/3***	***−5/3***
											−1	***0***	***1***
	4	6.805	8.507	11.325	86.26	78.53	82.57	−45.76	127.31		1	0	0
											0	1	0
											0	0	1
6	1	5.588	10.865	12.660	88.88	89.49	82.00	−46.05	126.84	$Z = 3$, $n = 1$	1	0	0
											1	1	1
											0	−1	1
	2	8.499	8.598	10.884	88.81	74.79	84.08	−45.94	127.15		1	0	0
											0	1	0
											0	0	1
	3	8.498	8.573	10.917	74.34	87.33	84.91	−45.90	127.11		1	0	0
											0	1	0
											0	0	1
	4	***6.369***	***10.774***	***11.451***	***101.90***	***86.29***	***97.10***	***−45.82***	***127.08***	***Z = 1, n = 1***	***2/3***	***1/3***	***1/3***
											−1/3	***1/3***	***7/3***
											0	***−1***	***1***
	5	6.880	8.552	14.021	102.01	76.20	81.12	−45.74	127.56	$Z = 3$, $n = 4$	1	0	0
											0	0	1
											1	−2	0
	6	6.429	11.135	11.307	108.71	91.53	87.70	−45.66	127.73	$Z = 1$, $n = 2$	−1/2	1/2	−1
											1/2	1/2	−2
											−1/2	−3/2	−1
	7	6.377	11.223	11.288	71.88	87.84	86.81	−45.62	127.74		1/2	1/2	0
											−1/2	1/2	−1
											−1/2	3/2	0

[a] Minimized experimental structure found by the DSM is shown with bold italic font, in a different, but equivalent, representation from the one usually used; see section 6 and also footnotes *d* and *e*. [b] The number of the successive lowest-energy local-minimum structure for given *Z*. [c] Shows equivalent unit cell with lowest possible *Z* in the present table. [d] The lattice vectors in the current line can be expressed as linear combinations of the lattice vectors of the probable lattice (shown in Table 6) with the elements of the standard equivalence matrix; i.e, the product of the lattice vectors from Table 6 and the standard matrix produces a set of lattice vectors whose parameters are very close to those in the current line. [e] For an example of how to show the agreement between the lattice parameters of the equivalent structures, see Appendix A.

The question of how to improve the potential is not a subject of this paper, but it is apparent that the methods introduced here can be used as a tool for testing and refining a potential.

Benzene crystallizes with four molecules in the unit cell of an orthorhombic lattice.[52,53] The parameters of the unit cell of the experimental structure are $a = 7.357$, $b = 9.373$, $c = 6.701$ Å. After energy minimization with the AMBER potential, these values became $a = 7.431$, $b = 9.167$, $c = 6.605$ Å. The DEM was applied with one, two, three, four, or eight molecules, using the AMBER potential. The computations revealed the minimized experimental structure with four or eight molecules (see Table 3, $Z = 4$, $n = 1$ and $Z = 8$, $n = 1$). The lowest energies obtained with one, two, or three molecules were higher than those obtained with four or eight molecules.

The DSM was applied to benzene with the same numbers of molecules. As with the DEM, the DSM found the minimized experimental structure with four or eight molecules (see Table 5, $Z = 4$, $n = 1$ and $Z = 8$, $n = 1$); the lowest energies obtained with one, two, or three molecules were higher. Consequently, the value of $Z = 4$ and the structure $Z = 4$, $n = 1$ is chosen as the predicted crystal structure. By contrast to the calculations on hexasulfur, few higher-energy artifacts were found.

There is good agreement between the predicted and experimental benzene crystal structures. The predicted unit cell is orthorhombic with *Pbca* symmetry (see Table 7), and discrepancies between the experimental and the predicted crystal-structure lattice-vector lengths, *a*, *b*, and *c*, are 1.0%, 2.2%, and 1.4%, respectively (see Tables 3 and 5). The 87° angle between the planes of the benzene molecules in the experimental crystal structure[15,52,53] (the so-called edge-to-face[15] arrangement of molecules) is predicted correctly. There is also good agreement between our three lowest-energy structures for benzene ($Z = 4$, $n = 1$; $Z = 2$, $n = 1$; $Z = 2$, $n = 2$ of Tables 3, 5, and 7) and the structures obtained by Gibson and Scheraga[30] and by Dzyabchenko.[54,55]

The minimized experimental crystal structure of hexasulfur ($Z = 3$) located by both methods, the DSM and the DEM, is shown in Figure 1. The predicted crystal structure of benzene is presented in Figure 2. Figure 3 shows the lowest-energy structures for hexasulfur ($Z = 3$) and benzene ($Z = 4$), corresponding to the most deformed potentials by the DSM (i.e., when the deformation parameter α is the largest).

7. Pressure Dependence for Benzene

All of the above computations were carried out with no pressure term included in the total energy function. Since benzene crystallizes differently when pressure is applied, we reminimized several lowest-energy structures (listed in Table 5) with the pressure correction term of Busing and Matsui[56] included, and the results are shown in Table 8. The reference volume V_0 was taken as 112.49 Å^3/mol, the volume of the minimized experimental lattice. The high-pressure structures are geometrically close to their low-pressure counterparts, but, depending on the applied pressure, the energetic order of the minima changes (Figure 4). The results of the local minimizations at 25 kbar are shown in Table 8, together with the standard equivalence matrix for the lowest-energy structure.

8. Space-Group Symmetry of Computed Structures

Tables 6 and 7 list the probable space-group symmetry of the calculated structures of S_6 and benzene, respectively,

TABLE 5: Parameters of Calculated Structures for C_6H_6 Crystals Using the DSM[a]

Z	n[b]	a (Å)	b (Å)	c (Å)	α (deg)	β (deg)	γ (deg)	energy (kcal/mol)	volume of unit cell (Å^3/mol)	equivalence indicator[c]	standard equivalence matrix[d,e]		
1	1	4.860	4.860	4.860	86.51	86.51	86.51	−11.91	114.21		2/3	1/3	1/3
											−1/3	1/3	1/3
											−1/3	−2/3	1/3
	2	5.199	5.199	5.256	77.83	77.83	115.73	−11.73	117.49		1/2	1/2	0
											1/2	−1/2	0
											0	0	−1
2	1	5.511	6.264	6.751	90.00	90.00	73.12	−13.78	111.50		−1	0	0
											−1	0	−1
											0	−1	0
	2	5.421	5.496	7.641	90.00	74.07	90.00	−13.51	109.47		1	0	0
											0	−1	0
											0	0	−1
	3	5.435	6.489	7.790	66.06	90.00	114.74	−13.07	111.62		0	1	0
											1/2	−1/2	0
											0	0	−1
	4	5.567	5.567	7.923	103.52	103.52	81.20	−12.89	115.17		−1/2	−1/2	0
											−1/2	1/2	0
											0	0	−1
	5	5.487	6.374	7.163	90.00	90.00	64.52	−12.63	113.08		1	0	0
											0	0	−1
											0	1	0
3	1	5.412	9.190	9.190	63.76	101.32	78.68	−12.74	126.88		0	0	−1
											−1/3	1/3	−1/3
											1/3	2/3	1/3
	2	5.355	6.283	10.674	81.69	89.74	71.98	−12.71	112.53		1	0	0
											0	1	0
											0	0	1
	3	5.412	5.416	11.901	89.21	81.05	87.22	−12.67	114.72		1	0	0
											0	1	0
											0	0	1
4	***1***	***6.605***	***7.431***	***9.167***	***90.00***	***90.00***	***90.00***	***−13.88***	***112.49***		***0***	***0***	***1***
											1	***0***	***0***
											0	***1***	***0***
	2	6.752	7.039	9.469	97.65	90.00	90.00	−13.79	111.50	$Z = 2$, $n = 1$	0	−1	0
											0	0	−1
											2	0	1
	3	7.719	7.719	8.065	73.18	106.82	89.21	−13.51	109.47	$Z = 2$, $n = 2$	−1	−1	0
											1	−1	0
											1	0	1
8	***1***	***6.605***	***9.168***	***14.861***	***90.00***	***90.00***	***90.00***	***−13.88***	***112.48***	***Z = 4, n = 1***	***0***	***0***	***1***
											0	***1***	***0***
											−2	***0***	***0***
	2	7.039	9.470	13.502	90.00	90.00	97.65	−13.79	111.50	$Z = 2$, $n = 1$	0	0	−1
											2	0	1
											0	−2	0
	3	6.586	7.310	18.705	86.49	90.00	90.00	−13.73	112.37		0	1	0
											1	0	0
											0	0	−1

[a] Minimized experimental structure found by the DSM is shown with bold italic font, in a different, but equivalent, representation from the one usually used; see section 6 and also footnotes *d* and *e*. [b] The number of the successive lowest-energy local-minimum structure for given *Z*. [c] Shows equivalent unit cell with lowest possible *Z* in the present table. [d] The lattice vectors in the current line can be expressed as linear combinations of the lattice vectors of the probable lattice (shown in Table 7) with the elements of the standard equivalence matrix; i.e, the product of the lattice vectors from Table 7 and the standard matrix produces a set of lattice vectors whose parameters are very close to those in the current line. [e] For an example of how to show the agreement between the lattice parameters of the equivalent structures, see Appendix A.

deduced by methods described elsewhere.[30] These have several features of interest. First, although both molecules have $\bar{3}$ symmetry, there is a marked scarcity of rhombohedral or trigonal space groups in either table. Both molecules did pack in $R\bar{3}$ structures in the computations with $Z = 1$; this corresponded to the experimentally observed structure for S_6 but not for benzene. The only other rhombohedral structure was the $R3$ lattice obtained with benzene with $Z = 3$, which had nine molecules rather than three in the (trigonal) unit cell. There is also a paucity of orthorhombic structures, namely, one each for S_6 and benzene (the latter corresponding to the experimentally observed *Pbca* low-pressure structure). By contrast, there is a large number of triclinic lattices, especially for S_6; the majority of these had $P\bar{1}$ symmetry, although one $P1$ structure was obtained in each case. The remainder of the structures fall into common classes of monoclinic primitive or centered space groups.

Another point of interest concerns the two lowest-energy packings of S_6 and benzene when the unit cell contained one molecule (Tables 4, 3, and 5, respectively). In both cases, the molecules in the lowest-energy structure were arranged in layers of hexagonal arrays with their mean planes parallel to the *C* face, the molecules in adjacent layers being offset in a manner consistent with rhombohedral centering. Also, in both cases, the molecules in the next lowest-energy structure were arranged in rows lying parallel to the *b* axis in the *C* face, with their

TABLE 6: Probable Space-Group Symmetry of the Calculated S_6 Structures

equivalent structures	Z^a	N^b	a (Å)	b (Å)	c (Å)	α (deg)	β (deg)	γ (deg)	space group
Tab.4 $Z = 1$, $n = 1$; Tab.4 $Z = 2$, $n = 1$ Tab.4 $Z = 3$, $n = 3$; Tab.2 $Z = 3$, $n = 3$ Tab.4 $Z = 4$, $n = 1$; Tab.4 $Z = 5$, $n = 3$ Tab.4 $Z = 6$, $n = 4$; Tab.2 $Z = 6$, $n = 4$	3	1/6	10.816	10.816	3.765	90.00	90.00	120.00	$R\bar{3}$
Tab.4 $Z = 1$, $n = 2$; Tab.4 $Z = 3$, $n = 5$ Tab.4 $Z = 4$, $n = 2$; Tab.4 $Z = 6$, $n = 6$	2	1/4	10.892	6.578	3.769	90.00	108.98	90.00	$C2/m$
Tab.4 $Z = 1$, $n = 3$; Tab.4 $Z = 2$, $n = 4$ Tab.4 $Z = 3$, $n = 7$; Tab.2 $Z = 3$, $n = 7$ Tab.4 $Z = 4$, $n = 4$	1	1/2	4.189	5.705	6.182	67.67	70.36	88.65	$P\bar{1}$
Tab.4 $Z = 1$, $n = 4$	2	1/4	7.458	6.630	5.603	90.00	111.11	90.00	$C2/m$
Tab.4 $Z = 2$, $n = 2$	2	1/2	6.031	6.848	6.798	90.00	114.59	90.00	$P2_1/c$
Tab.4 $Z = 2$, $n = 3$	4	1/2	10.934	6.586	7.098	90.00	90.00	90.00	$Cmc2_1$
Tab.4 $Z = 2$, $n = 5$	4	1/2	9.938	7.446	7.059	90.00	95.59	90.00	$C2/c$
Tab.4 $Z = 3$, $n = 1$; Tab.2 $Z = 3$, $n = 1$ Tab.4 $Z = 6$, $n = 1$; Tab.2 $Z = 6$, $n = 1$	3	1 and 1/2	5.588	8.493	8.614	95.47	103.30	104.27	$P\bar{1}$
Tab.4 $Z = 3$, $n = 2$; Tab.2 $Z = 3$, $n = 2$	3	1 and 1/2	5.560	8.528	8.558	95.83	103.42	101.79	$P\bar{1}$
Tab.4 $Z = 3$, $n = 4$; Tab.2 $Z = 3$, $n = 4$ Tab.4 $Z = 6$, $n = 5$	3	1 and 1/2	6.880	7.034	8.552	73.57	81.12	75.45	$P\bar{1}$
Tab.2 $Z = 3$, $n = 6$	3	1 and 1/2	5.518	8.413	8.511	82.91	99.12	83.63	$P\bar{1}$
Tab.4 $Z = 3$, $n = 6$; Tab.2 $Z = 3$, $n = 5$ Tab.2 $Z = 6$, $n = 6$	3	1 and 1/2	6.889	7.000	8.497	75.30	81.73	76.07	$P\bar{1}$
Tab.4 $Z = 4$, $n = 3$	2	1/2	6.358	11.030	3.768	90.00	105.09	90.00	$P2_1/n$
Tab.4 $Z = 5$, $n = 1$[c]	5	2 and 1/2	8.005	8.006	10.783	73.44	73.45	95.18	$P\bar{1}$
Tab.4 $Z = 5$, $n = 2$	5	2 and 1/2	6.796	8.516	11.325	85.73	78.70	82.39	$P\bar{1}$
Tab.4 $Z = 5$, $n = 4$	5	5	6.805	8.507	11.325	86.26	78.53	82.57	$P1$
Tab.4 $Z = 6$, $n = 2$; Tab.2 $Z = 6$, $n = 2$	6	2 and 2(1/2)[d]	8.499	8.598	10.884	88.81	74.79	84.08	$P\bar{1}$
Tab.4 $Z = 6$, $n = 3$; Tab.2 $Z = 6$, $n = 3$	6	3	8.498	8.573	10.917	74.34	87.33	84.91	$P\bar{1}$
Tab.4 $Z = 6$, $n = 7$[e]	3	1/2 and 1/4[f]	10.922	6.586	11.454	90.00	111.53	90.00	$C2/m$
Tab.2 $Z = 6$, $n = 5$[g]	2	2(1/4)	10.935	6.591	8.938	90.00	127.50	90.00	$C2/m$
Tab.4 $Z = 2$, $n = 6$	2	2	5.763	6.380	8.136	102.38	94.84	114.65	$P1$

[a] Number of molecules in the probable unit cell. [b] Number of molecules in the probable asymmetric unit. [c] Normals to the mean planes of all molecules lie in planes parallel to the (1, 1, 0) plane and make an angle of 34.8° with the *c* axis; centers of three molecules lie on a line from (0, 0, 0) to (1, 1, 1), and centers of the remaining two lie on parallel line through (1/2, 1/2, 1/2); all molecules are related by inversion but not by crystallographic rotation or reflection. [d] Asymmetric unit consists of two whole molecules and two unrelated half-molecules. [e] Lattice consists of layers of a *C*2/*m* lattice with four molecules in the unit cell and $^1/_2$ molecule in the asymmetric unit, alternating with layers of a *C*2/*m* lattice with two molecules in the unit cell and $^1/_4$ molecule in the asymmetric unit; inversion points of these two lattices are at (0, 0, 0) and (0, 1/2, 1/2), respectivley. [f] Asymmetric unit consists of unrelated half-molecule and 1/4 molecule. [g] Lattice consists of alternating layers of two unrelated *C*2/*m* lattices with two molecules in the unit cell and $^1/_4$ molecule in the asymmetric unit, and inversion points at (0, 0, 0) and (0, 1/2, 1/2), respectively.

mean planes perpendicular to the *C* face and with adjacent rows offset in a manner consistent with *C*-face centering.

Perhaps the greatest interest attaches to the triclinic $P\bar{1}$ packings of S_6 and benzene. All but two of the $P\bar{1}$ structures of S_6, together with the single $P\bar{1}$ packing of benzene, involve packings that are physically rather improbable, since their asymmetric units contain one or more half-molecules plus one or more whole molecules. Each half-molecule is related by inversion through the origin to the other half of either the same molecule or one of its translational images, and each whole molecule is related by inversion in a similar way to another whole molecule. The whole molecules and half-molecules in these packings are crystallographically unrelated. Regarded as regular packings of disjoint points in space, such arrangements of atoms are perfectly legitimate; however, it is difficult to see how a real crystal could be nucleated and built up from identical molecules whose environments differ so significantly. These packings are geometrically reasonable but physically unreasonable. This argument does not apply to the $P\bar{1}$ structure of S_6 that was obtained when $Z = 1$, because in that packing all molecules would experience the same environment. Another implausible packing, for much the same reason, is the *C*2/*m* structure of S_6 obtained by the DSM with six molecules (Table 4, $Z = 6$, $n = 7$). As noted in footnote *f* of Table 6, this structure can be generated by merging alternate layers of a *C*2/*m* structure with four molecules in the unit cell and $^1/_2$ molecule in the asymmetric unit, and another *C*2/*m* structure with two molecules in the unit cell and $^1/_4$ molecule in the asymmetric unit. Again, it is very difficult to see how such a structure would be nucleated. Structures such as the ones discussed here must be regarded as artifacts of the computational method, which relies entirely on energy minimization and takes no account of the process by which the crystal is formed. The *relative* energies of the physically plausible and implausible structures could presumably be changed by adjusting the parameters of the potential, but this may not eliminate the implausible structures; therefore, the existence of such artifactual structures should probably be accepted as due to the incompleteness of the thermodynamic function. In the calculations with S_6, two artifactual packings (for each of three, five, and six molecules, respectively, in the unit cell) were found that had lower energies than the experimentally observed packing; however, the ex-

TABLE 7: Probable Space-Group Symmetry of the Calculated Benzene Structures

equivalent structures	Z^a	N^b	a (Å)	b (Å)	c (Å)	α (deg)	β (deg)	γ (deg)	space group
Tab.3 $Z = 1$, $n = 1$; Tab.5 $Z = 1$, $n = 1$	3	1/6	6.661	6.661	8.916	90.00	90.00	120.00	$R\bar{3}$
Tab.3 $Z = 1$, $n = 2$; Tab.5 $Z = 1$, $n = 2$	2	1/4	5.530	8.804	5.255	90.00	113.35	90.00	$C2/m$
Tab.3 $Z = 2$, $n = 1$; Tab.5 $Z = 2$, $n = 1$ Tab.3 $Z = 4$, $n = 2$; Tab.5 $Z = 4$, $n = 2$ Tab.3 $Z = 8$, $n = 2$; Tab.5 $Z = 8$, $n = 2$	2	1/2	5.511	6.751	7.040	90.00	121.63	90.00	$P2_1/c$
Tab.3 $Z = 2$, $n = 2$; Tab.5 $Z = 2$, $n = 2$ Tab.3 $Z = 4$, $n = 3$; Tab.5 $Z = 4$, $n = 3$	2	1/2	5.421	5.497	7.641	90.00	105.93	90.00	$P2_1/c$
Tab.5 $Z = 2$, $n = 3$	4	1/2	11.788	5.435	7.791	90.00	116.55	90.00	$C2/c$
Tab.5 $Z = 2$, $n = 4$	4	2(1/2)[c]	8.453	7.246	7.923	90.00	107.94	90.00	Cm
Tab.3 $Z = 2$, $n = 3$; Tab.5 $Z = 2$, $n = 5$	2	1/2	5.487	7.163	6.374	90.00	115.48	90.00	$P2_1/m$
Tab.3 $Z = 3$, $n = 1$; Tab.5 $Z = 3$, $n = 1$	9	1	15.608	15.608	5.412	90.00	90.00	120.00	$R3$
Tab.3 $Z = 3$, $n = 2$; Tab.5 $Z = 3$, $n = 2$	3	1 and 1/2	5.355	6.283	10.674	81.69	89.74	71.98	$P\bar{1}$
Tab.3 $Z = 3$, $n = 3$; Tab.5 $Z = 3$, $n = 3$	3	3	5.412	5.416	11.901	89.21	81.05	87.22	$P1$
Tab.3 $Z = 4$, $n = 1$; Tab.5 $Z = 4$, $n = 1$ Tab.3 $Z = 8$, $n = 1$; Tab.5 $Z = 8$, $n = 1$	4	1/2	7.431	9.167	6.605	90.00	90.00	90.00	$Pbca$
Tab.5 $Z = 8$, $n = 3$	8	4	18.705	6.586	7.310	90.00	93.51	90.00	Pc

[a] Number of molecules in the probable unit cell. [b] Number of molecules in the probable asymmetric unit. [c] Asymmetric unit consists of two unrelated half-molecules.

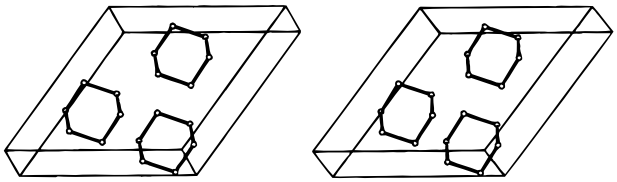

Figure 1. Minimized experimental structure for hexasulfur found by the DEM and the DSM ($a = b = 10.816$ Å, $c = 3.764$ Å, $\alpha = \beta = 90°$, $\gamma = 120°$).

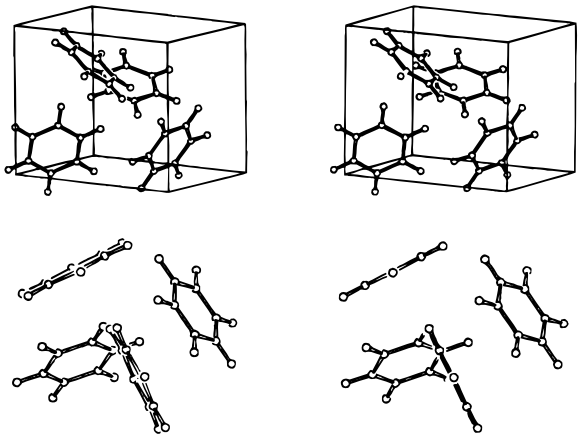

Figure 2. (a, top) Predicted crystal structure of benzene found by the DEM and the DSM ($Z = 4$, $n = 1$ from Table 5; $a = 6.605$ Å, $b = 7.431$ Å, $c = 9.167$ Å, $\alpha = \beta = \gamma = 90.00°$). (b, bottom) Details of edge-to-face arrangement of benzene molecules.

perimentally observed crystal structure is still among the lowest-energy ones computed.

9. Conclusions

We have presented two methods for global minimization, both based on the idea of using a smoothing transformation of the original potential surface, and recovering the deepest minima of the original energy function by a reversing procedure when the transformation is gradually removed. Both methods proved to be extremely powerful, not only in solving problems that are considered very difficult[1,2] but also in solving the even more

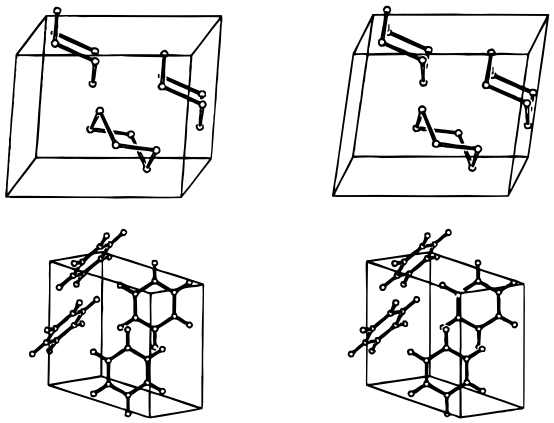

Figure 3. Lowest-energy structures corresponding to the most deformed potentials using the DSM for (a, top) hexasulfur ($Z = 3$; $a = 5.407$ Å, $b = 8.113$ Å, $c = 8.241$ Å, $\alpha = 93.78°$, $\beta = 75.72°$, $\gamma = 76.06°$) and (b, bottom) benzene ($Z = 4$; $a = b = 7.317$ Å, $c = 7.363$ Å, $\alpha = \beta = 101.50°$, $\gamma = 90.30°$).

difficult problem that arises when the number of molecules in the unit cell, and consequently the number of variables, is doubled.

To demonstrate the high performance of the DEM and the DSM, 500 randomly started local minimizations were carried out for S_6 with six molecules and for C_6H_6 with eight molecules without using any deformation of the potential function. None of them reached a structure with energy close to the global-minimum structure, despite an enormous computational expense, considerably greater than the computational costs of the DEM and the DSM runs.

The excellent performance is due not only to the smoothing transformations but also to the essential use of several trajectories coupled with a mechanism (described in section 2) that determines whether to maintain or to discard a structure at a given transformation level.

The results show that the AMBER potential which was used to simulate the interactions between benzene molecules leads to the experimentally observed crystal structures at low and high pressures. The minimized experimental crystal structures of benzene are the global-minima structures of the potential for all pressures considered here. However, the potential that was

TABLE 8: Parameters of Locally Minimized Structures of C_6H_6 Crystals at 25 kbar[a]

Z	*n*[b]	*a* (Å)	*b* (Å)	*c* (Å)	α (deg)	*β* (deg)	*γ* (deg)	energy (kcal/mol)	volume of unit cell (Å^3/mol)	standard equivalence matrix[c,d]		
4	***3***	***7.501***	***7.501***	***7.766***	***72.00***	***108.00***	***89.00***	***−17.06***	***98.05***	***1***	***−1***	***0***
										−1	***−1***	***0***
										−1	***0***	***−1***
	2	6.091	8.366	8.366	79.00	100.71	79.29	−16.60	100.05			
	1	6.214	7.247	8.971	90.00	90.00	90.00	−16.36	101.00			

[a] Minimized experimental structure found by the DSM is shown with bold italic font, in a different, but equivalent, representation from the one usually used; see section 6 and also footnotes *c* and *d*. [b] The structures in this table are listed as succesive lowest-energy local-minimum structures (at 25 kbar); the number *n* indicates the structure from Table 5 being minimized locally at 25 kbar. [c] The lattice vectors in the current line can be expressed as linear combinations of the lattice vectors of the minimized experimental structure for benzene at 25 kbar ($Z = 2$, $a = 5.258$ Å, $b = 5.350$ Å, $c = 7.209$ Å, $\alpha = 90.00°$, $\beta = 104.74°$, $\gamma = 90.00°$), with the coefficients of the standard equivalence matrix; the minimized experimental structure for benzene at 25 kbar reported in ref 14, where different potential parameters were used, agrees closely with the above ($Z = 2$, $a = 5.424$ Å, $b = 5.521$ Å, $c = 7.432$ Å, $\alpha = 90.00°$, $\beta = 105.90°$, $\gamma = 90.00°$). [d] For an example of how to show the agreement between the lattice parameters of the equivalent structures, see Appendix A.

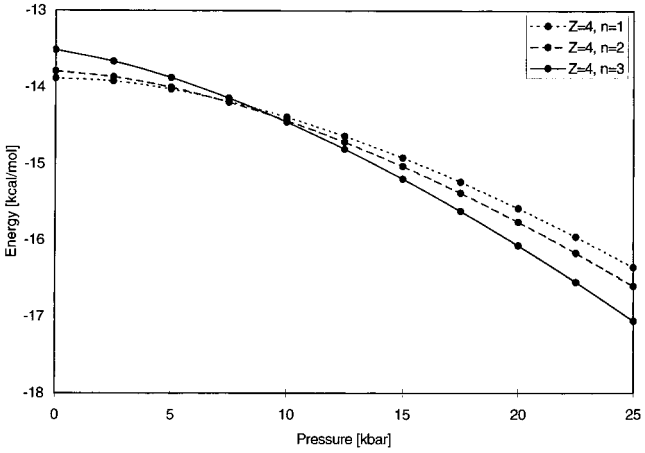

Figure 4. Results for energy minimizations of crystals of benzene at various pressures for $Z = 4$ and $n = 1$, 2, and 3, respectively.

used for S_6 molecules is not accurate enough to allow the proper prediction, unless a number of lower-energy artifacts that could probably not be observed are discarded on physical grounds.

Both methods can be applied to crystals consisting of any rigid molecule with a dipole moment equal to zero. A molecule with a nonzero dipole moment may lead to a unit cell with a nonzero dipole moment; however, the very definition of the energy of a polar crystal is still unclear.[19,20,23] Consequently, the definition of the energy of a crystal consisting of flexible, charged molecules is still under investigation. We are currently using the DEM and the DSM to try to treat crystals of flexible molecules with dipole moments. Attempts are also being made to reduce the CPU time required by our algorithms (see section 10).

Since both methods have also been applied with considerable success in other global-optimization problems, unrelated to crystal structure prediction,[37−40,42] they seem to be well-suited to a broad spectrum of very different applications in physical chemistry.

A great advantage of the DSM is the very simple way in which it is applied, compared to the DEM. Instead of complicated formulas for convolutions, spline techniques, etc., we use a simple algebraic formula (eq 2). At the same time, the behavior of the DSM is practically the same as that of the DEM. This simplicity allows for immediate and straightforward application of the DSM to individual flexible molecules and to crystals of flexible molecules.

10. Computations

The computations were carried out in parallel on an IBM SP2 cluster containing 512 nodes (at the Cornell University Theory Center). The programs were parallelized on the fine grain level by using the IBM Message-Passing Interface, distributing the pairwise interactions in the function and gradient computations among the processors; 30−50 processors were usually used. The overhead in the parallel computations did not exceed 20% for these numbers of processors.

An average CPU time for one randomly started local minimization with the original (untransformed) potential was 3418 CPU seconds for six S_6 molecules and about 7 CPU hours for eight benzene molecules (all timings are reported as if the computations were carried out on one processor); these averages are calculated from the test of 500 randomly started local minimizations, which did not reveal any structures energetically close to the global minimum. The runs with the DEM or the DSM consumed a CPU time equivalent to about 100 randomly started local minimizations (with the undeformed potential) for both hexasulfur and benzene molecules. A single local minimization with the deformed potential costs up to 20 times less than that with the original potential because the shape of the deformed surface is simpler, and the minimization procedure needs fewer iteration steps.

Appendix A

As an example, we show how the parameters (a, b, c, α, β, γ) of the calculated unit cell of the S_6 crystal structure $Z = 3$, n=3 of Table 4 agree with the lattice parameters of the minimized experimental structure (a lattice with three molecules in a trigonal unit cell; the first structure in Table 6). The Cartesian coordinates (a_1, a_2, a_3, b_1, b_2, b_3, c_1, c_2, c_3,) of the lattice vectors can be calculated by using the following formulas: $a_1 = a$, $a_2 = a_3 = 0$; $b_1 = b\cdot\cos\gamma$, $b_2 = b\cdot\sin\gamma$, $b_3 = 0$; $c_1 = c\cdot\cos\beta$, $c_2 = (b\cdot c\cdot\cos\alpha - b_1\cdot c_1)/b_2$, $c_3 = (c^2 - c_1^2 - c_2^2)^{1/2}$. For the trigonal lattice, $a = b = 10.816$ Å, $c = 3.765$ Å, $\alpha = \beta = 90°$, $\gamma = 120°$, and the Cartesian coordinates become $a_1 = 10.816$, $a_2 = a_3 = 0.0000$; $b_1 = -5.4080$, $b_2 = 9.3669$, $b_3 = 0.0000$; $c_1 = 0.0000$, $c_2 = 0.0000$, $c_3 = 3.7650$. Multiplying the matrix of these Cartesian coordinates by the standard equivalence matrix from Table 4, a set of Cartesian coordinates is obtained, which should be a representation of the lattice vectors of the structure $Z = 3$, $n = 3$:

$$\begin{bmatrix} 1/3 & 2/3 & 2/3 \\ 1/3 & -1/3 & 2/3 \\ 2/3 & 1/3 & -5/3 \end{bmatrix} \cdot \begin{bmatrix} 10.8160 & 0.0000 & 0.0000 \\ -5.4080 & 9.3669 & 0.0000 \\ 0.0000 & 0.0000 & 3.7650 \end{bmatrix} =$$

$$\begin{bmatrix} 0.0000 & 6.2446 & 2.5100 \\ 5.4080 & -3.1223 & 2.5100 \\ 5.4080 & 3.1223 & -6.2750 \end{bmatrix}$$

Indeed, the lengths of the resulting vectors **a**, **b**, **c** calculated from these Cartesian coordinates are 6.7302, 6.7302, and 8.8527,

respectively, and agree with the lengths in Table 4 ($Z = 3$, $n = 3$). Similarly, the angles α, β, γ are: 86.38°, 86.38°, and 106.95° and agree with the angles in Table 4.

Acknowledgment. This work was supported by grants from the National Science Foundation (MCB 95-13167) and the National Institute of General Medical Sciences of the National Institutes of Health (GM-14312). Support was also received from the Association for International Cancer Research and the Cornell Biotechnology Center. The computations were carried out on the IBM SP2 Supercomputer at the Cornell National Supercomputer Facility, a resource of the Cornell Center for Theory and Simulation in Science and Engineering, which receives major funding from the National Science Foundation and the IBM Corporation, with additional support from New York State and members of its Corporate Research Institute, and from the National Center for Research Resources of the National Institutes of Health. We thank N. Jourdan for helpful discussions.

References and Notes

(1) Maddox, J. *Nature* **1988**, *335*, 201.
(2) Gavezzotti, A. *Acc. Chem. Res.* **1994**, *27*, 309.
(3) Gavezzotti, A.; Filippini, G. *J. Am. Chem. Soc.* **1995**, *117*, 12299.
(4) Gavezzotti, A. *J. Am. Chem. Soc.* **1991**, *113*, 4622.
(5) Karfunkel, H. R.; Gdanitz, R. J. *J. Comput. Chem.* **1992**, *13*, 1171.
(6) Gdanitz, R. J. *Chem. Phys. Lett.* **1992**, *190*, 391.
(7) Perlstein, J. *J. Am. Chem. Soc.* **1992**, *114*, 1955.
(8) Karfunkel, H. R.; Rohde, B.; Leusen, F. J. J., Gdanitz, R. J.; Rihs, G. *J. Comput. Chem.* **1993**, *14*, 1125.
(9) Perlstein, J. *J. Am. Chem. Soc.* **1994**, *116*, 455.
(10) Perlstein, J. *Chem. Mater.* **1994**, *6*, 319.
(11) Perlstein, J. *J. Am. Chem. Soc.* **1994**, *116*, 11420.
(12) Williams, D. E. *Acta Crystallogr.* **1996**, *A52*, 326.
(13) Gavezzotti, A.; Filippini, G. *J. Am. Chem. Soc.* **1996**, *118*, 7153.
(14) Gavezzotti, A. *Acta Crystallogr.* **1996**, *B52*, 201.
(15) Chaka, A. M.; Zaniewski, R.; Youngs, W.; Tessier, C.; Klopman, G. *Acta Crystallogr.* **1996**, *B52*, 165.
(16) Ewald, P. P. *Ann. Phys. (Leipzig)* **1921**, *64*, 253.
(17) Nijboer, B. R. A.; De Wette, F. W. *Physica* **1957**, *XXIII*, 309.
(18) Catti, M. *Acta Crystallogr.* **1978**, *A34*, 974.
(19) De Leeuw, S. W.; Perram, J. W.; Smith, E. R. *Proc. R. Soc. London* **1980**, *A373*, 27.
(20) Smith, E. R. *Proc. R. Soc. London* **1981**, *A375*, 475.
(21) Deem, M. W.; Newsam, J. M.; Sinha, S. K. *J. Phys. Chem.* **1990**, *94*, 8356.
(22) Figueirido, F.; Del Buono, G. S.; Levy, R. M. *J. Chem. Phys.***1995**, *103*, 6133.
(23) Van Eijck; B. P.; Kroon, J. *J. Phys. Chem. B* **1997**, *101*, 1096.
(24) Price, S. L. *J. Chem. Soc., Farady Trans.* **1996**, *92*, 2997.
(25) Coombes, D. S.; Price, S. L.; Willock, D. J.; Leslie, M. *J. Phys. Chem.* **1996**, *100*, 7352.
(26) Sorescu, D. C.; Rice, B. M.; Thompson, D. L. *J. Phys. Chem. B* **1997**, *101*, 798.
(27) Filippini, G.; Gavezzotti, A. *Acta Crystallogr.* **1993**, *B49*, 868.
(28) Gavezzotti, A.; Filippini, G *J. Phys. Chem.* **1994**, *98*, 4831.
(29) Gibson, K. D.; Scheraga, H. A. *J. Phys. Chem.* **1995**, *99*, 3752.
(30) Gibson, K. D.; Scheraga, H. A. *J. Phys. Chem.* **1995**, *99*, 3765.
(31) Weiner, S. J.; Kollman, P. A.; Nguyen D. T.; Case, D. A. *J. Comput. Chem.* **1986**, *7*, 230.
(32) Busing, W. R. *WMIN, A Computer Program to Model Molecules and Crystals in Terms of Potential Energy Functions*; ORNL-5747; Oak Ridge National Laboratory: Oak Ridge, TN, 1981.
(33) Williams, D. E. *QCPE Bull.* **1984**, *4*, 82.
(34) Van Eijck, B. P.; Mooij, W. T. M.; Kroon, J. *Acta Crystallogr.* **1995**, *B51*, 99.
(35) Kitaigorodskii, A. I. *Bull. Acad. Sci. URSS, Cl. Sci. Chim.* **1946**, 587.
(36) Pannetier, J.; Bassas-Alsina, J.; Rodriguez-Carvajal, J.; Caignaert, V. *Nature* **1990**, *346*, 343.
(37) Piela, L.; Kostrowicki, J.; Scheraga, H. A. *J. Phys. Chem.* **1989**, *93*, 3339.
(38) Kostrowicki, J.; Piela, L.; Cherayil, B. J.; Scheraga, H. A. *J. Phys. Chem.* **1991**, *95*, 4113.
(39) Kostrowicki, J.; Scheraga, H. A. *J. Phys. Chem.* **1992**, *96*, 7442.
(40) Wawak, R. J.; Wimmer, M. M.; Scheraga, H. A. *J. Phys. Chem.* **1992**, *96*, 5138.
(41) Wawak, R. J.; Gibson, K. D.; Liwo, A.; Scheraga, H. A. *Proc. Natl. Acad. Sci. U.S.A.* **1996**, *93*, 1743.
(42) Pillardy, J.; Piela, L. *J. Phys. Chem.* **1995**, *99*, 11805.
(43) Shao, C.-S.; Byrd, R. H.; Eskow, E.; Schnabel, R. B. *Global Optimization for Molecular Clusters Using a New Smoothing Approach, The IMA Volumes in Mathematics and its Applications, Volume 94, Large Scale Optimization with Applications, Part III: Molecular Structure and Optimization*; Biegler, L. T., Coleman, T. F., Conn, A. R., Santosa, F. N., Eds.; Springer-Verlag: New York, 1997; pp 163−199.
(44) Pillardy, J.; Olszewski, K. A.; Piela, L. *J. Phys. Chem.* **1992**, *96*, 4337.
(45) Pillardy, J.; Olszewski, K. A.; Piela, L. *J. Mol. Struct.: THEOCHEM* **1992**, *270*, 277.
(46) Li, Z.; Scheraga, H. A. *Proc. Natl. Acad. Sci. U.S.A.* **1987**, *84*, 6611.
(47) Li, Z.; Scheraga, H. A. *J. Mol. Struct.: THEOCHEM* **1988**, *179*, 333.
(48) Gay, D. M. *ACM Trans. Math. Software* **1983**, *9*, 503.
(49) Szmydt, Z. *Fourier Transformation and Linear Differential Equations*; D. Reidel Publishing Company: Dordrecht, Holland/Boston, MA, 1977.
(50) Press, W. H.; Teukolsky, S. A.; Vetterling, W. T.; Flannery, B. P. *Numerical Recipes in FORTRAN, The Art of Scientific Computing*, 2nd ed.; Cambridge University Press: Cambridge, 1992, p 107.
(51) Donohue, J.; Caron, A.; Goldish, E. *J. Am. Chem. Soc.* **1961**, *83*, 3748.
(52) Bacon, G. E.; Curry, N. A.; Wilson, S. A. *Proc. R. Soc. London, Ser. A* **1964**, *279*, 98.
(53) Jeffrey, G. A.; Ruble, J. R.; McMullan, R. K.; Pople, J. A *Proc. R. Soc. London, Ser. A* **1987**, *414*, 47.
(54) Dzyabchenko, A. V. *J. Struct. Chem.* **1984**, *25*, 416.
(55) Dzyabchenko, A. V. *Sov. Phys. Crystallogr.* **1989**, *34*, 131.
(56) Busing, W. R.; Matsui, M. *Acta Crystallogr.* **1984**, *A40*, 532.